European Journal of Pharmaceutics and Biopharmaceutics 76 (2010) 120–126

Contents lists available at ScienceDirect

European Journal of Pharmaceutics and Biopharmaceutics

journal homepage: www.elsevier.com/locate/ejpb

Research paper

Bisphosphonate protonation states, conformations, and dynamics on bone mineral probed by solid-state NMR without isotope enrichment

Matthew S. Ironside [a], Melinda J. Duer [a,*], David G. Reid [a], Stephen Byard [b]

[a] Department of Chemistry, University of Cambridge, Cambridge, United Kingdom
[b] Department of Analytical Sciences, Sanofi-Aventis, Northumberland, United Kingdom

ARTICLE INFO

Article history:
Received 3 February 2010
Accepted in revised form 25 May 2010
Available online 8 June 2010

Keywords:
Drug targeting
Biomaterials
Chemical shift anisotropy
REDOR
Molecular dynamics
Osteoporosis

ABSTRACT

Recognition of bone mineral by bisphosphonates is crucial to their targeting, efficacy, therapeutic and diagnostic applications, and pharmacokinetics. In a search for rapid and simple NMR approaches to assessing the bone recognition characteristics of bisphosphonates, we have studied alendronate, pamidronate, neridronate, zoledronate and tiludronate, in crystalline form and bound to the surface of pure bone mineral stripped of its organic matrix by a simple chemical process. ^{31}P NMR chemical shift anisotropies and asymmetries in the crystalline compounds cluster strongly into groupings corresponding to fully protonated, monoprotonated, and deprotonated phosphonate states. All the mineral-bound bisphosphonates cluster in the same anisotropy–asymmetry space as the deprotonated phosphonates. In ^{13}C{^{31}P} rotational echo double resonance (REDOR) experiments, which are sensitive to carbon–phosphorus interatomic distances, the strongly mineral-bound alendronate displays very similar conformational and side chain dynamics to its crystalline state. Pamidronate and neridronate, with shorter and longer sidechains, respectively, and generally weaker mineral binding, display more dynamical sidechains in the mineral-bound state. The REDOR experiment provides a simple rationalization of bisphosphonate-mineral affinity in terms of molecular structure and dynamics, consistent with findings from much more labour- and time-intensive isotope labelling approaches.

1. Introduction

Bisphosphonates (typified by the structures of the bisphosphonates in this study in Fig. 1) provide an important drug therapy for diseases of inappropriate bone resorption, including osteoporosis, myelomas and bone metastases, and Paget's disease of bone [1]. Moreover, their ability to bind highly selectively to bone mineral in the mammalian body has meant that, conjugated to other actives, they also have actual and potential uses as vehicles for bone targeting of therapeutic and imaging radioisotopes, antibacterials, and antineoplastics [2]. Their use in treating chronic resorptive diseases like osteoporosis relies on relatively long-term binding of the bisphosphonate molecules to bone mineral and subsequent interference with the cellular processes of bone resorbing osteoclasts [3–6]; their interactions with the target farnesyl pyrophosphate synthetase (FPPS) have been studied by NMR [7]. Their beneficial effect in demineralizing diseases may also be partly attributable to inhibition of osteoblast apoptosis [8,9]. Weaker bone-binding molecules also have clinical usefulness [10] and indeed there are contexts, such as in pediatric use, in which strong bone binding may actually be undesirable.

There is thus intense interest in developing methods to probe the nature of the bisphosphonate–bone mineral recognition and binding mechanisms [11,12]. In particular, recent solid-state NMR studies have given crucial insight into how several bisphosphonate species bind to human bone material and their conformations and dynamics [13,14]. These studies depend on ^{13}C, ^{15}N and ^{2}H labelled bisphosphonates bound to untreated human bone; the isotopic enrichment of the bisphosphonates allowed their respective NMR signals to be visible against the background of natural abundance signals arising from organic components in the bone, primarily type I collagen. Enrichment enabled ^{13}C{^{15}N} TEDOR (transferred echo double resonance) experiments to probe the conformations of the bone-bound bisphosphonates, and ^{2}H NMR their dynamics. Such approaches involving multiple syntheses of stable isotope-enriched compounds, while extremely elegant, are not practical for screening new bisphosphonates for mineral binding propensity and characteristics within the demanding timescales of a commercial drug discovery or development programme.

The main impediment to applying solid-state NMR to study the structural aspects of bisphosphonate-bone recognition is (as

* Corresponding author. Address: Department of Chemistry, University of Cambridge, Cambridge CB2 1EW, United Kingdom. Tel.: +44 0 1223 336483; fax: +44 0 1223 336362.
E-mail addresses: Matt.Ironside@cantab.net (M.S. Ironside), Mjd13@cam.ac.uk (M.J. Duer), Dgr30@cam.ac.uk (D.G. Reid), Stephen.Byard@sanofi-aventis.com (S. Byard).

0939-6411/$ - see front matter © 2010 Elsevier B.V. All rights reserved.
doi:10.1016/j.ejpb.2010.05.013

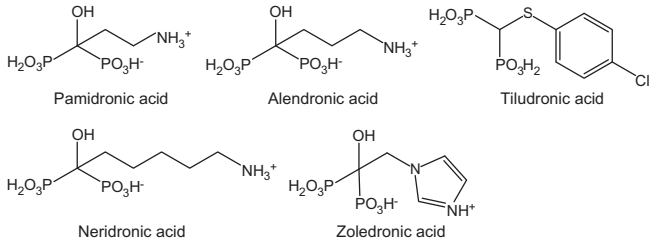

Fig. 1. Chemical structural formulae of the five bisphosphonates studied.

already alluded to) the strong natural abundance signals from bone biopolymers. Another method besides isotope enrichment of circumventing this is by studying bisphosphonates complexed with synthetic hydroxyapatites [12], and thermodynamic insights into binding affinities have been obtained in this way [11]. However synthetic hydroxyapatites do not closely mimic native bone mineral in several respects. First, they do not reproduce the numerous substitutions of different biological cations (e.g. sodium, magnesium) and anions (e.g. carbonate, chloride) into the ideal ($Ca_{10}(PO_4)_6(OH)_2$) structure. Second, and probably more importantly, the surface of bone, the structure of which is clearly a crucial determinant of bisphosphonate binding, is more heterogeneous, hydrated, and poorly ordered than typical synthetic hydroxyapatites [15,16] and is certainly not well represented by the surface of the latter.

There is ample evidence that bisphosphonates bind to bone mineral *via* the two phosphonate groups and possibly also *via* the hydroxyl group (when present) on carbon 1 [17,18]. The enthalpy of binding *via* the phosphonate groups is clearly dependent on their charge and thus protonation state; the hydroxyl group is more likely to be involved in hydrogen bonding to mineral surface entities. In bisphosphonates with a terminal amine group, there is evidence that this group also binds to the bone mineral [19], anchoring the bisphosphonate molecular conformation, which affects the entropy of binding. There are thus two features of particular importance when screening the bone mineral-binding properties of a new bisphosphonate: (i) the protonation state of the phosphonate groups when the molecule is bound to bone mineral and (ii) the conformation of the bound molecule. Quantum mechanical calculations [20] have suggested that the ^{31}P chemical shift tensor of the phosphonate groups is highly sensitive to protonation state, in contrast to the chemical shift. $^{13}C\{^{31}P\}$ REDOR spectra of bisphosphonate bound to mineral in intact bone would, of course, be dominated by signals from the organic matrix in bone (primarily collagen), making the much smaller signals from the bisphosphonate difficult to extract with any certainty.

In this work, we present a straightforward method of determining the protonation state of the phosphonate groups in mineral-bound bisphosphonates, by measurements of ^{31}P chemical shift anisotropies, and show how $^{13}C\{^{31}P\}$ REDOR can be used to examine the conformation of bone mineral-bound bisphosphonate, using natural abundance levels of ^{13}C. The organic matrix is not strongly relevant to studies of molecules binding to bone *mineral;* and hence in this work, we use bone from which the organic matrix has been removed by chemical digestion. Powder X-ray diffraction (pXRD), ^{31}P NMR, and two-dimensional ^{1}H–^{31}P heteronuclear correlation spectra [15,21] show that the resulting bone mineral is broadly similar to that in intact bone, suggesting that it represents a realistic substrate for examining the binding of bisphosphonates. Furthermore, our $^{13}C\{^{31}P\}$ REDOR results lead to conclusions in agreement with those of the earlier $^{13}C\{^{15}N\}$ TEDOR study utilizing labelled bisphosphonates on intact bone [14], again suggesting that our relatively simple approach produces meaningful and valuable results.

2. Materials and methods

2.1. Bone mineral

Bone mineral was produced from equine bone by powdering the bone in a laboratory ball mill and then digesting the powder for several weeks in concentrated sodium hydroxide and sodium hypochlorite to remove the organic collagenous matrix. The free mineral was then filtered, washed thoroughly with distilled water, dried in air, and stored at −20 °C. Loss of collagen and other matrix macromolecules was confirmed by their disappearance from the ^{13}C CP-MAS NMR spectrum.

2.2. Bisphosphonates

Monosodium alendronate trihydrate, disodium pamidronate, and neridronic acid were purchased from Sigma. Disodium tiludronate was synthesized by Sanofi-Aventis using described procedures [22]. Disodium zoledronate was donated by Novartis. All compounds were used without further purification.

2.3. Mineral-bound bisphosphonates

Bisphosphonates (ca. 0.1 mmol) were dissolved in ca. 5 ml water and pH adjusted to neutral with dilute NaOH or HCl; neridronic acid was sparingly soluble in water but was solubilized by addition of the base. To each solution about 100 mg of dry bone mineral was added, the mixture was allowed to stand overnight at 4 °C, filtered, washed several times with distilled water to remove bisphosphonate not strongly bound to mineral surface, and the resultant bisphosphonate–bone mineral complexes dried in air at room temperature.

2.4. NMR measurements

All experiments were performed on a Bruker 400 MHz Avance spectrometer operating at a ^{1}H frequency of 400.1 MHz, ^{31}P frequency of 161.9 MHz and ^{13}C frequency of 100.5 MHz.

^{31}P chemical shift anisotropy measurements were made on one-dimensional CP-MAS spectra of all the bisphosphonates in the spectra of which structurally inequivalent ^{31}P signals are well resolved, at MAS rates between 4 and 6 kHz. CP from ^{1}H to ^{31}P was effected with a 2.5 μs ^{1}H $\pi/2$ pulse followed by 5 ms ^{1}H-^{31}P cross-polarization contact, then high-power TPPM ^{1}H decoupling with a field strength of 100 kHz during acquisition. The exception is pamidronate (in the ^{31}P spectrum of which two structurally inequivalent signals are fortuitously overlapped) for which the powder–sideband correlation pattern approach [23] was used. Here, the ^{31}P MAS-CSA spectrum of pamidronate was recorded at a spinning rate of 5750 Hz and with the CSA-recoupling sequence in t_1 having an anisotropic scaling factor of $\chi a = 0.1797$, giving an ω_1 spectral width of 32 kHz. The basic CSA-recoupling pulse unit in t_1 consisted of six π-pulses in three rotor periods. There were 20 $t1$ complex data points collected, with 150 scans per point using a cogwheel phase cycling scheme [24]. The ^{1}H–^{31}P ramped cross-polarization contact time was 5 ms with a ^{1}H field strength of 78 kHz. The ^{31}P π-pulse length was 5.9 μs, and the ^{1}H $\pi/2$-pulse length was 3.2 μs. High-power TPPM proton decoupling was applied throughout with a field strength of 78 kHz. Recycle delays of 6 s and 2 s, respectively, were used for the crystalline and for the mineral-bound materials.

$^{13}C\{^{31}P\}$ REDOR measurements were performed on a standard Bruker triple-resonance magic-angle-spinning probe using 4-mm zirconia rotors. Samples were packed in the middle one-third of the rotor, the rest of the rotor being packed with Teflon tape. For

alendronate and neridronate, the sample spinning rate was 12.5 kHz; for pamidronate, it was 8 kHz. The ^{1}H $\pi/2$ pulse length was 2.5 μs, ^{1}H–^{13}C cross-polarization contact time, 4 ms and the ^{31}P π-pulse length, 8.1 μs. High-power TPPM ^{1}H decoupling was applied with a field strength of 100 kHz. The number of rotor cycles of the REDOR sequence was varied to give the dephasing times shown in the figures. The number of scans was also varied between experiments, the effect of which is seen in the error bars. The recycle delay was 2 s for mineral-bound bisphosphonates and 6 s for crystalline bisphosphonates, with the exception of pamidronate for which it was 10 s for the pure crystalline material. To construct the dephasing curves, the intensity was integrated over the peak widths shown in the figures, and the ratio of the dephased intensity to the reference intensity was calculated. The errors were calculated from the standard deviation in the noise.

3. Results and discussion

3.1. ^{31}P chemical shift anisotropy measurements

Chemical shift anisotropy (CSA) has its origin in the fact that the NMR shielding of a given atomic nucleus is a function of local electronic structure and distribution, which in turn depends on the molecular scaffold surrounding it, and the orientation of this scaffold with respect to the external polarizing (B_0) field of the NMR magnet (see any solid-state NMR textbook such as Duer [25] for a discussion of theory and relationship of CSA to molecular structure). The CSA characteristics of every NMR-active nucleus in a solid are a fundamental property of the structure of that solid and can give valuable insights into this structure. Moreover, the CSA is fairly easy to extract from simple non-overlapped spectra, such as those of all the crystalline bisphosphonates studied except pamidronate, by side band analysis at moderate spinning speeds. It is convenient to define the CSA in terms of three parameters, the (familiar) isotropic chemical shift δ_{iso} (which is what is observed in the standard MAS experiment), an anisotropy ζ (in units of ppm), and a dimensionless asymmetry parameter η; ζ and η are effectively independent of δ_{iso} and so are useful parameters for comparing the CSA characteristics of nuclei with different δ_{iso}.

The ^{31}P chemical shift anisotropies and asymmetries for the crystalline bisphosphonates shown in Fig. 1 were measured as described elsewhere [26–28] and are shown in Table 1 (error estimates in parentheses are Cramer-Rao upper bounds [29]). The protonation state of all these bisphosphonates in their crystalline form is known from X-ray diffraction structural analysis [30,31] or is obvious from their counterion stoichiometry. Fig. 2 shows a scatter plot of chemical shift anisotropy ζ versus asymmetry η; there is a clear correlation between these chemical shift parameters and protonation state, and these clusterings are colour coded. Moreover, the groupings are very well separated, so that knowledge of the chemical shift anisotropy and asymmetry should allow a confident assignment of protonation state.

Bisphosphonate–bone mineral complexes give rise to a single broad bisphosphonate ^{31}P NMR signal at about 20 ppm (relative to 85% phosphoric acid at 0 ppm) and well resolved from the ^{31}P signal from bone mineral itself (between 2 and 3 ppm). ^{31}P spectra of the mineral-bound bisphosphonates are compared to those of the respective crystalline bisphosphonates in Fig. 3; they are very similar to those already published [12,14], with the bisphosphonates contributing a single broad signal to high frequency of the mineral signal. Table 2 lists the room temperature chemical shift anisotropies and asymmetries measured for these bisphosphonates bound to native bone.

Of course in whole bone, there is a significant possibility that native organic matrix components will compete with pharmacological bisphosphonates for mineral binding and that therefore our experiments using stripped bone mineral are unrepresentative. To address this important point, we repeated all the experiments just described with a complex formed between zoledronate and native bone; results were indistinguishable from those obtained on the zoledronate–mineral complex suggesting that the organic matrix in native bone is not an effective competitor for bisphosphonate-binding sites. Moreover, in order to rule out the possibility that molecular dynamics of a mineral-bound bisphosphonate at room temperature are partially averaging the shielding interaction, the measurements were repeated at 273 K for alendronate, zoledronate, and tiludronate and at 223 K for zoledronate; no differences in the chemical shift parameters were detected, suggesting that the phosphonate groups at least are static on the NMR timescale.

Table 1
Experimental ^{31}P chemical shift parameters for the five crystalline bisphosphonates studied. δ_{iso} – Isotropic chemical shift referenced to external 85% phosphoric acid at 0 ppm; ζ – chemical shift anisotropy; η – asymmetry. These are defined as follows in terms of the three principal values of the chemical shielding tensor δ_{xx}, δ_{yy} and δ_{zz}: $\delta_{iso} = 1/3(\delta_{xx} + \delta_{yy} + \delta_{zz})$; $\zeta = \delta_{zz} - \delta_{iso}$; $\eta = (\delta_{xx} - \delta_{yy})/\zeta$. See Ref. [23] for an extensive discussion of the fitting procedures and the estimation of the Cramer-Rao upper bound error limits shown in parentheses.

Bisphosphonate	Protonation state	δ_{iso} (ppm)	ζ (ppm)	η
Pamidronate (disodium)	De	20.5	68.0 (0.1)	0.24 (0.01)
	Mono	20.5	−83.2 (0.2)	0.99 (0.01)
Alendronate (monosodium)	Mono	22.1	69.9 (0.2)	0.72 (0.01)
	Mono	17.4	−77.4 (0.4)	0.88 (0.02)
Neridronate (free acid)	Bis	23.9	−60.1 (0.2)	0.54 (0.02)
	Bis	21.6	−66.9 (0.2)	0.46 (0.02)
	Mono	18.2	53.2 (0.2)	0.83 (0.02)
	Mono	12.1	64.0 (0.1)	0.96 (0.01)
Zoledronate (disodium)	Mono	17.1	−80.4 (0.8)	0.99 (0.02)
	Mono	13.8	78.4 (0.4)	0.84 (0.01)
	De	10.7	74.8 (0.4)	0.35 (0.02)
	De	8.7	73.5 (0.4)	0.55 (0.02)
Tiludronate (disodium)	Mono	20.8	−75.3 (0.2)	0.90 (0.02)
	Mono	17.2	−71.6 (0.6)	0.97 (0.02)

Both the chemical shift anisotropy and asymmetry fall within a relatively narrow range for all the mineral-bound bisphosphonates studied, corresponding to the region expected for the fully deprotonated state. It would seem therefore that the primary factor affecting the chemical shift anisotropy and asymmetry in these molecules is their protonation state. Other factors, such as molecular structure, degree of hydrogen bonding, and other inter/intramolecular interaction must have an effect of course, but these considerations would seem to play a more minor role. This is not surprising. In terms of geometrical structure, the phosphonate geometry is unlikely to deviate significantly from tetrahedral around the ^{31}P. In terms of electronic structure, the electron distribution in the P–O bonds will be most influenced by the net charge on the phosphonate group which in turn is dominated by the protonation state.

3.2. $^{13}C\{^{31}P\}$ REDOR measurements

The rotational echo double resonance (REDOR) experiment is a powerful technique for obtaining a measure of interatomic distances in crystalline and non-crystalline solids [32]. Briefly, the method recouples the through-space interaction between nuclear magnetic dipoles, which is usually removed in conventional solid-state NMR experiments by magic-angle-spinning because it is a significant source of spectral broadening and degrades resolution. This is effected by applying a series of rotor-synchronized radiofrequency pulses at the resonance frequency of one of the interacting elements (^{31}P in this case) while observing the signals from the other (^{13}C in this instance). In practice, the experiment is

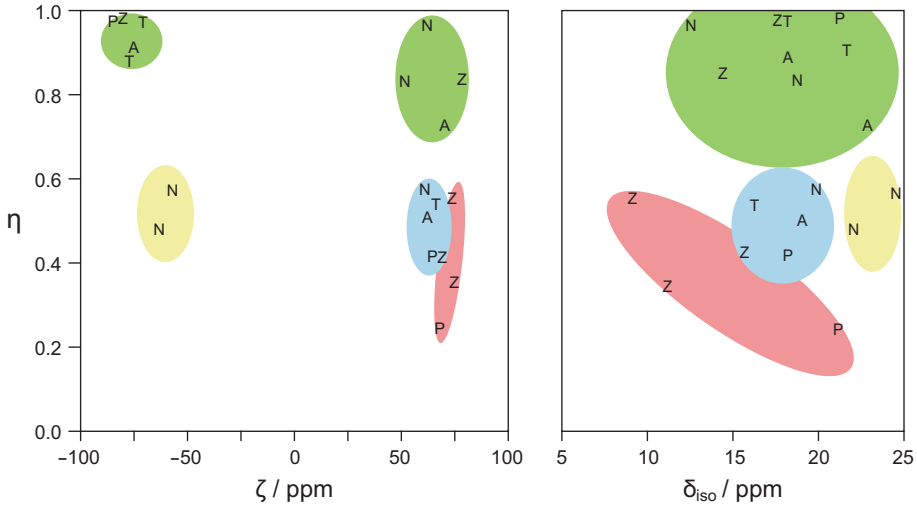

Fig. 2. Scatter plot of the distributions of ^{31}P chemical shift asymmetry (η) against anisotropy (ζ) (left hand panel) and against isotropic chemical shift (δ_{iso}) (right hand panel). The colour coded regions correspond to the state of the relevant phosphonate group as follows: red – fully deprotonated, green – monoprotonated, yellow – bis-protonated; the blue regions correspond to mineral-bound bisphosphonates. Individual compounds are identified by letters on the scatter plots as follows: A – monosodium alendronate; P – disodium pamidronate; N – neridronic acid; Z – disodium zoledronate; T – disodium tiludronate. (For interpretation of the references to colour in this figure legend, the reader is referred to the web version of this article.)

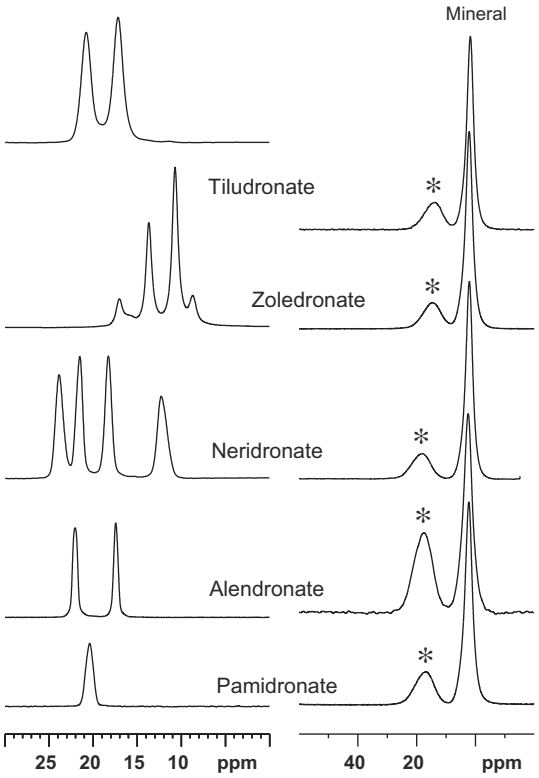

Fig. 3. ^{31}P CP-MAS spectra of the crystalline bisphosphonates (left hand traces) and spectra of the respective bisphosphonates bound to bone mineral (right hand traces) in which the single broad bisphosphonate signal is asterisked. (Crystalline disodium zoledronate is a mixture of two distinct hydrate forms, which accounts for the signal multiplicity.)

performed in two stages; a reference spectrum is acquired without the ^{31}P–^{13}C coupling, then a REDOR spectrum is acquired in which the rotor-synchronized pulses on the ^{31}P channel have restored this coupling. The effect is best appreciated by overlaying the reference and REDOR spectra. The internuclear dipole–dipole coupling manifests as a decrease in ^{13}C intensity on the part of those

Table 2
Experimental ^{31}P chemical shift parameters for the five bisphosphonates bound to bone mineral. Symbols have the same meaning as in Table 1. Quoted values are means, which are likely to reflect some range of values due to heterogeneity of binding geometry.

Bisphosphonate complexed to bone mineral	δ_{iso} (ppm)	ζ (ppm)	η
Pamidronate	17.5	64.5 (0.4)	0.42 (0.04)
Alendronate	18.5	62.2 (0.4)	0.50 (0.02)
Neridronate	19.1	61.0 (0.6)	0.57 (0.04)
Zoledronate	15.2	69.8 (0.6)	0.41 (0.04)
Tiludronate	15.7	65.8 (0.8)	0.53 (0.04)

^{13}C signals in close proximity to ^{31}P, a phenomenon referred to as dephasing. The dipole–dipole coupling between two neighbouring spins is inversely proportional approximately to the sixth power of the distance between them, and the dependence of the amount of dephasing on recoupling time can, in favourable cases of isolated spin pairs, be analyzed to yield accurate interatomic distances. The 100% natural abundance and high NMR receptivity of the NMR-active ^{31}P isotope of phosphorus makes it a particularly attractive, non-perturbing, and readily available REDOR "probe" nucleus of interatomic distances, and hence potentially molecular conformation and intermolecular interactions, in biological and pharmacological systems where it is naturally present [15,33]. It makes the REDOR method particularly attractive in qualitative and comparative investigations into the conformation and mechanisms of action of the bisphosphonates. Quantitative analysis is challenging, however, and has not been pursued, because the presence of two ^{31}P spins in any bisphosphonate structure means that as far as phosphorus–carbon interactions are concerned the ideal "isolated spin pair" condition is never fulfilled. Moreover, in the crystalline materials at least, the presence of intermolecular as well as intramolecular dipole–dipole interactions introduces a further level of complexity. Rationalizing the REDOR behaviour quantitatively for any of the crystals is not within the scope of this work.

Alendronate, pamidronate, and neridronate all bind to bone mineral, with alendronate binding most strongly and neridronate least [1,6]. As they only differ by the length of the carbon chain between the phosphonate groups and terminal amine, they represent a useful homologous series to gain some insight into the factors, which affect the strength of binding.

3.2.1. Alendronate

Typical $^{13}C\{^{31}P\}$ REDOR data are shown in Fig. 4, obtained on crystalline monosodium alendronate and alendronate bound to bone mineral. Dephasing curves for the ^{13}C sites in crystalline alendronate and alendronate bound to bone mineral derived by digesting native bone are shown in Fig. 5. Even without reference to the X-ray crystal structure of alendronate [30], the dephasing characteristics of each carbon atom relative to one another are consistent with structure; $^{13}C\{^{31}P\}$ REDOR curves simulated according to the ^{13}C–^{31}P intramolecular distances determined from this structure agree well with the experimental curve for the crystalline compound (not shown). As Fig. 5 shows, there is a high degree of similarity between the experimental REDOR curve for the pure crystalline material and that for the mineral-bound molecule. This suggests a very similar molecular geometry in both cases; and moreover, no molecular dynamics on the NMR timescale, as any reorientational motion of the molecule or part of it would reduce the effective ^{13}C–^{31}P dipolar couplings and result in slower dephasing on the REDOR curves. This suggests that the bisphosphonate not only binds via the phosphonate groups but also binds via the terminal amine group, anchoring the molecular conformation. Presumably in solution, prior to binding, the C_3 chain of the alendronate molecule is relatively mobile, so binding to bone mineral and consequent loss of this mobility constitutes a significant loss of entropy.

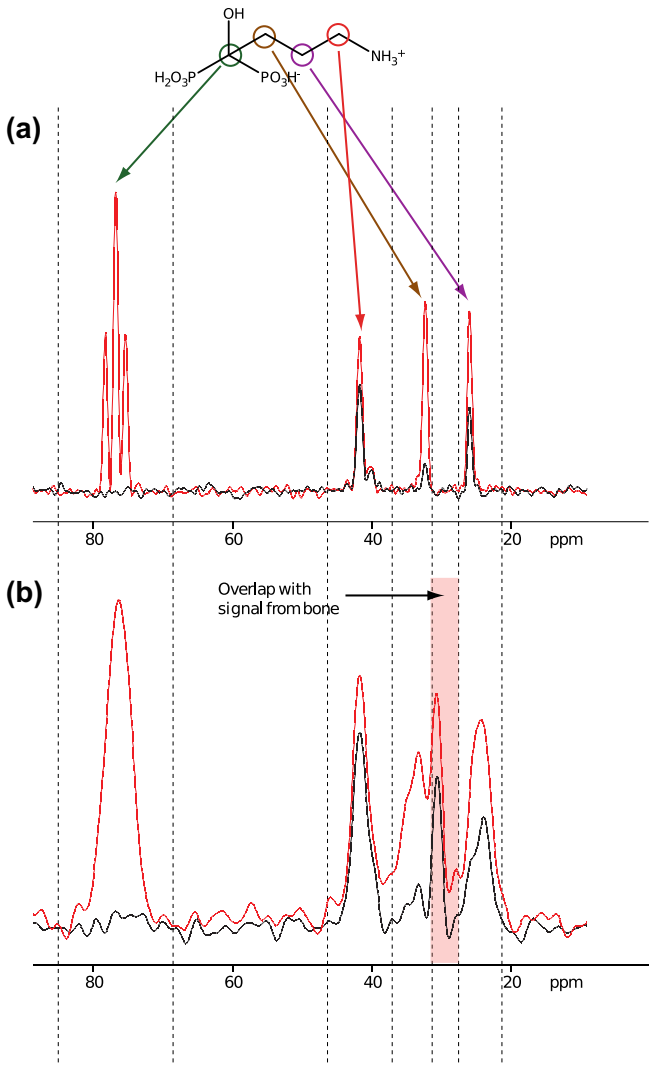

Fig. 4. $^{13}C\{^{31}P\}$ REDOR data from crystalline monosodium alendronate (top) and alendronate bound to bone mineral (bottom). Each red trace is a reference ^{13}C spectrum acquired with the ^{31}P–^{13}C through-space magnetic dipole–dipole interaction inactive, while each black trace was acquired under identical conditions to the red trace which it overlays, except that the phosphorus–carbon dipole–dipole interaction is activated by the REDOR procedure (for 2.6 ms in each case shown). Signals from structurally different carbon atoms lose intensity, i.e. dephase, under REDOR recoupling to a greater or lesser extent depending on whether they are close to or distant from neighbouring phosphorus atoms. Dashed vertical lines represent low field and high field limits between which integration of individual peaks was performed. The region in the spectrum from bone mineral highlighted in red contains the signal from lipid included in the mineral, which does not respond to REDOR and which was excluded from the integrals of the bisphosphonate peaks. (For interpretation of the references to colour in this figure legend, the reader is referred to the web version of this article.)

3.2.2. Pamidronate

The $^{13}C\{^{31}P\}$ REDOR dephasing curves for pamidronate in pure and mineral-bound form are shown in Fig. 6. Mukherjee et al. [14] propose that the carbon chain in bone-bound pamidronate adopts a *gauche* conformation, presumably so that the terminal amine group can interact with the mineral surface as well as the phosphonate groups. The REDOR dephasing curves in Fig. 6 shows strong similarity between the crystalline pamidronate (crystal structure [31]) and mineral-bound pamidronate for all ^{13}C except C-3, which shows slightly more rapid dephasing in the initial part of the REDOR curve than in the crystalline form, which would be expected if the mineral-bound molecule does indeed adopt a *gauche* conformation, although the difference between the curves is relatively small within the level of error. If such a conformation does indeed occur, it would explain why pamidronate binds less strongly to bone mineral than alendronate. The large differences between the curves for the crystalline and mineral-bound molecules for C-2 are largely due to the fact that the ^{13}C signal for this site is overlapped with a residual lipid signal from the bone mineral in the mineral-bound form, so extraction of the C-2 signal intensity with any degree of certainty is difficult.

3.2.3. Neridronate

$^{13}C\{^{31}P\}$ REDOR data for neridronic acid and mineral-bound neridronate are typified in Fig. 7, and derived dephasing curves are shown in Fig. 8. The crystal structure of the polymorph we are working with is unknown, but as Fig. 7a shows, there are (at least) two molecules in the asymmetric unit, as there are two signals for most ^{13}C sites. (Although a crystal structure for neridronic acid has been determined [34], its predicted X-ray powder diffractogram is inconsistent with that of the polymorph we are studying; data not shown.) The signals from C-4 and C-5 in the mineral-bound sample are overlapped with the residual lipid signal in the bone mineral and so the REDOR curves for these signals are impossible to extract with any degree of accuracy. Nevertheless, the REDOR dephasing curves from the other ^{13}C sites provide very useful information. C-3, C-6, and to some extent C-2 show much slower dephasing for the mineral-bound molecule than the crystalline form, suggesting significantly weaker ^{13}C–^{31}P dipolar couplings in the mineral-bound molecule than in the pure crystalline form. This is consistent with the terminal amine being unbound, or bound in a manner which still leaves the hydrocarbon chain relatively free to move, resulting in partially averaged ^{13}C–^{31}P dipolar couplings. The enthalpy penalty of poor amine binding might help explain why neridronate binds much less strongly to bone than alendronate and pamidronate. As for why the terminal amine

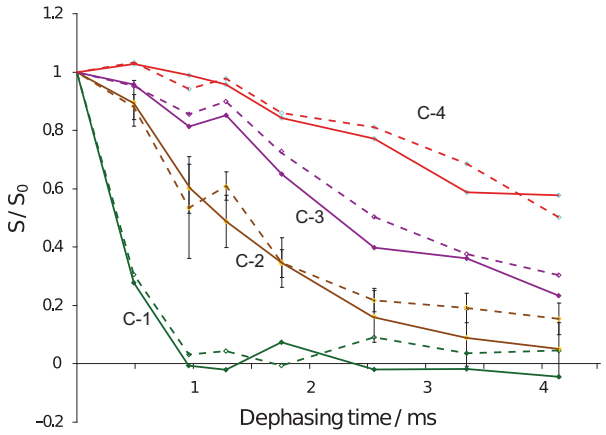

Fig. 5. $^{13}C\{^{31}P\}$ REDOR dephasing curves for crystalline monosodium alendronate (solid lines) and for alendronate bound to bone mineral (dashed lines). Curves are colour coded as follows: green C-1, brown C-2, mauve C-3, red C-4. Each data value is the intensity of the respective signal in the REDOR spectrum (S) relative to its intensity in the reference spectrum acquired for the same dephasing time (S_0). For additional clarity, traces have been labelled with the respective carbon atom. (For interpretation of the references to colour in this figure legend, the reader is referred to the web version of this article.)

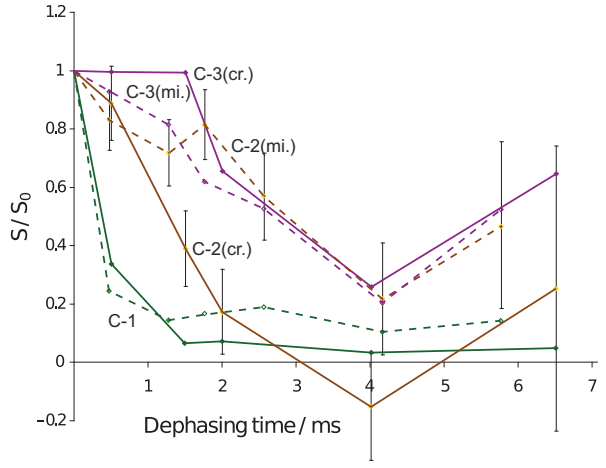

Fig. 6. $^{13}C\{^{31}P\}$ REDOR dephasing curves for crystalline disodium pamidronate (solid lines), and for pamidronate bound to bone mineral (dashed lines), colour coded as follows: green C-1, brown C-2, mauve C-3. Where necessary the labels on the traces distinguish between crystalline and mineral-bound signals with the suffixes (cr.) and (mi.), respectively. (For interpretation of the references to colour in this figure legend, the reader is referred to the web version of this article.)

group does not bind strongly on the NMR timescale, one surmises that it requires too greater a loss of entropy between the free molecule and that with both ends of the molecule bound to bone mineral.

Of course in all cases, it is possible that some of the observed $^{13}C\{^{31}P\}$ REDOR dephasing is attributable to dipole–dipole interactions between the ^{13}C of the bisphosphonate and ^{31}P in the bone mineral itself. While this possibility cannot be definitely excluded, its operation would serve to increase the dephasing in the mineral-bound bisphosphonates relative to that which is caused only by the intramolecular ^{13}C–^{31}P interactions operative in both crystalline and mineral-bound states. Even were mineral phosphate contributing to the overall REDOR dephasing seen in the mineral-bound bisphosphonates, the dephasing is still less than observed in the crystalline state, maintaining our overall conclusions about molecular dynamics.

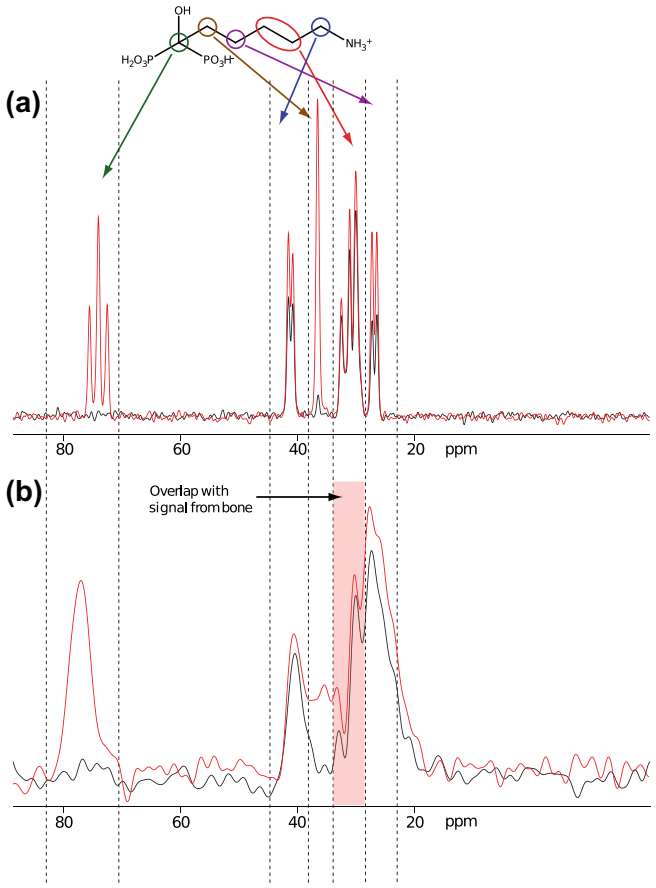

Fig. 7. $^{13}C\{^{31}P\}$ REDOR data from crystalline neridronic acid (top) and neridronate bound to bone mineral (bottom), at a dephasing time of 2.0 ms. Note the presence of two signals for most of the carbon atoms of crystalline neridronic acid signifying the presence of at least two non-equivalent structures in the crystallographic unit cell. (For interpretation of the references to colour in this figure legend, the reader is referred to the web version of this article.)

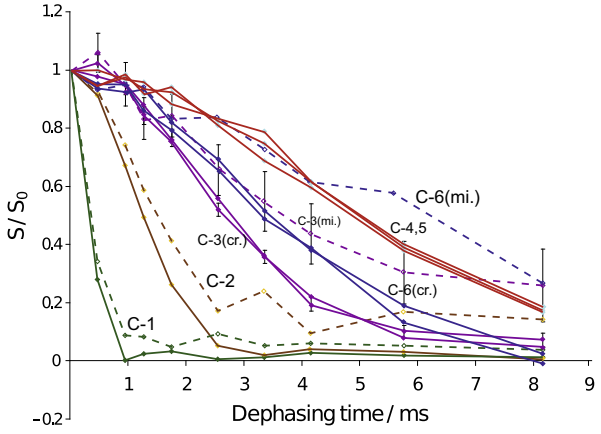

Fig. 8. $^{13}C\{^{31}P\}$ REDOR dephasing curves for crystalline neridronic acid (solid lines) and for neridronate bound to bone mineral (dashed lines), colour coded as follows: green C-1, brown C-2, mauve C-3, red C-4 and C-5 (unambiguous distinction not possible), blue C-6. The doubling of some traces from the crystalline material reflects the presence of two signals for the respective carbon. Measurements for C-4 and C-5 in the mineral-bound form were not possible due to overlap with the signal from residual lipid in the mineral. (For interpretation of the references to colour in this figure legend, the reader is referred to the web version of this article.)

4. Conclusions

This work has shown that bisphosphonates can be screened for their bone mineral-binding potential using relatively straightfor-

ward NMR techniques available, indeed routine, on many solid-state NMR instruments in academia, and increasingly within the pharmaceutical industry, without the need for isotope labelling or enrichment and using nanoparticulate bone mineral produced by a simple procedure digesting native bone so as to remove organic components. Bisphosphonates bind to bone mineral primarily via the phosphonate groups, and protonation state of these is readily determined by measurements of ^{31}P chemical shift anisotropy and asymmetry. Many bisphosphonates have one or more additional groups that can potentially bind to bone mineral. The involvement of these groups in binding can be assessed by ^{13}C{^{31}P} REDOR measurements on the mineral-bound bisphosphonate, which allows the structure of the molecular relative to its crystalline form to be compared and allows the determination of which groups are involved in any molecular motion in the mineral-bound bisphosphonate. The combination of these two factors allows ready assessment of which non-phosphonate groups are involved in binding the molecule to the bone mineral. These methods will assist in rapid screening of future bisphosphonates for their mineral-binding properties.

Acknowledgements

Dr. Rachel Murray (Animal Health Trust, UK) for equine bone, Dr. Jonathan Green (Novartis Pharma AG, Basel, Switzerland) for a gift of disodium zoledronate, the UK EPSRC (MSI) and BBSRC (DGR) for funding. The electron micrograph used in the graphical abstract was downloaded from the Bone Research Society website (http://www.brsoc.org.uk/gallery).

References

[1] R.G. Russell, Z. Xia, J.E. Dunford, U. Oppermann, A. Kwaasi, P.A. Hulley, K.L. Kavanagh, J.T. Triffitt, M.W. Lundy, R.J. Phipps, B.L. Barnett, F.P. Coxon, M.J. Rogers, N.B. Watts, F.H. Ebetino, Bisphosphonates: an update on mechanisms of action and how these relate to clinical efficacy, Ann. NY Acad. Sci. 1117 (2007) 209–257.
[2] S. Zhang, G. Gangal, H. Uludag, 'Magic bullets' for bone diseases: progress in rational design of bone-seeking medicinal agents, Chem. Soc. Rev. 36 (2007) 507–531.
[3] E. van Beek, E. Pieterman, L. Cohen, C. Lowik, S. Papapoulos, Farnesyl pyrophosphate synthase is the molecular target of nitrogen-containing bisphosphonates, Biochem. Biophys. Res. Commun. 264 (1999) 108–111.
[4] E. van Beek, E. Pieterman, L. Cohen, C. Lowik, S. Papapoulos, Nitrogen-containing bisphosphonates inhibit isopentenyl pyrophosphate isomerase/farnesyl pyrophosphate synthase activity with relative potencies corresponding to their antiresorptive potencies in vitro and in vivo, Biochem. Biophys. Res. Commun. 255 (1999) 491–494.
[5] J.E. Dunford, K. Thompson, F.P. Coxon, S.P. Luckman, F.M. Hahn, C.D. Poulter, F.H. Ebetino, M.J. Rogers, Structure-activity relationships for inhibition of farnesyl diphosphate synthase in vitro and inhibition of bone resorption in vivo by nitrogen-containing bisphosphonates, J. Pharmacol. Exp. Ther. 296 (2001) 235–242.
[6] R.G. Russell, N.B. Watts, F.H. Ebetino, M.J. Rogers, Mechanisms of action of bisphosphonates: similarities and differences and their potential influence on clinical efficacy, Osteoporos. Int. 19 (2008) 733–759.
[7] J.M. Sanders, A.O. Gomez, J. Mao, G.A. Meints, E.M. Van Brussel, A. Burzynska, P. Kafarski, D. Gonzalez-Pacanowska, E. Oldfield, 3-D QSAR investigations of the inhibition of Leishmania major farnesyl pyrophosphate synthase by bisphosphonates, J. Med. Chem. 46 (2003) 5171–5183.
[8] L.I. Plotkin, R.S. Weinstein, A.M. Parfitt, P.K. Roberson, S.C. Manolagas, T. Bellido, Prevention of osteocyte and osteoblast apoptosis by bisphosphonates and calcitonin, J. Clin. Invest. 104 (1999) 1363–1374.
[9] L.I. Plotkin, S.C. Manolagas, T. Bellido, Dissociation of the pro-apoptotic effects of bisphosphonates on osteoclasts from their anti-apoptotic effects on osteoblasts/osteocytes with novel analogs, Bone 39 (2006) 443–452.
[10] E.R. van Beek, C.W. Lowik, F.H. Ebetino, S.E. Papapoulos, Binding and antiresorptive properties of heterocycle-containing bisphosphonate analogs: structure–activity relationships, Bone 23 (1998) 437–442.
[11] G.H. Nancollas, R. Tang, R.J. Phipps, Z. Henneman, S. Gulde, W. Wu, A. Mangood, R.G. Russell, F.H. Ebetino, Novel insights into actions of bisphosphonates on bone: differences in interactions with hydroxyapatite, Bone 38 (2006) 617–627.
[12] G. Grossmann, A. Grossmann, G. Ohms, E. Breuer, R. Chen, G. Golomb, G. Cohen, G. Haegele, R. Classen, Solid-state NMR of bisphosphonates adsorbed on hydroxyapatite, Magn. Reson. Chem. 38 (2000) 11–16.
[13] S. Mukherjee, C. Huang, F. Guerra, K. Wang, E. Oldfield, Thermodynamics of bisphosphonates binding to human bone: a two-site model, J. Am. Chem. Soc. 131 (2009) 8374–8375.
[14] S. Mukherjee, Y. Song, E. Oldfield, NMR investigations of the static and dynamic structures of bisphosphonates on human bone: a molecular model, J. Am. Chem. Soc. 130 (2008) 1264–1273.
[15] M.J. Duer, T. Friscic, R.C. Murray, D.G. Reid, E.R. Wise, The mineral phase of calcified cartilage: its molecular structure and interface with the organic matrix, Biophys. J. 96 (2009) 3372–3378.
[16] S. Maltsev, M.J. Duer, R.C. Murray, C. Jaeger, A solid state NMR comparison of the mineral structure in bone from diseased joints of the horse, J. Mater. Sci. 42 (2007) 8804–8810.
[17] E. van Beek, M. Hoekstra, M. van de Ruit, C. Lowik, S. Papapoulos, Structural requirements for bisphosphonate actions in vitro, J. Bone Miner. Res. 9 (1994) 1875–1882.
[18] E. Van Beek, C. Lowik, I. Que, S. Papapoulos, Dissociation of binding and antiresorptive properties of hydroxybisphosphonates by substitution of the hydroxyl with an amino group, J. Bone Miner. Res. 11 (1996) 1492–1497.
[19] L. Widler, K.A. Jaeggi, M. Glatt, K. Muller, R. Bachmann, M. Bisping, A.R. Born, R. Cortesi, G. Guiglia, H. Jeker, R. Klein, U. Ramseier, J. Schmid, G. Schreiber, Y. Seltenmeyer, J.R. Green, Highly potent geminal bisphosphonates. From pamidronate disodium (Aredia) to zoledronic acid (Zometa), J. Med. Chem. 45 (2002) 3721–3738.
[20] J. Mao, S. Mukherjee, Y. Zhang, R. Cao, J.M. Sanders, Y. Song, Y. Zhang, G.A. Meints, Y.G. Gao, D. Mukkamala, M.P. Hudock, E. Oldfield, Solid-state NMR, crystallographic, and computational investigation of bisphosphonates and farnesyl diphosphate synthase–bisphosphonate complexes, J. Am. Chem. Soc. 128 (2006) 14485–14497.
[21] G. Cho, Y. Wu, J.L. Ackerman, Detection of hydroxyl ions in bone mineral by solid-state NMR spectroscopy, Science (New York, NY) 300 (2003) 1123–1127.
[22] J.C. Brelière, X. Emonds-Alt, G. Garcia, Produits anti-inflammatoires dérivés de l'acide méthylène diphosphonique et leur procédé de préparation, Eur. Pat. Appl. EP 100 (1984) 718.
[23] M.S. Ironside, D.G. Reid, M.J. Duer, Correlating sideband patterns with powder patterns for accurate determination of chemical shift parameters in solid-state NMR, Magn. Reson. Chem. 46 (2008) 913–917.
[24] M.H. Levitt, P.K. Madhu, C.E. Hughes, Cogwheel phase cycling, J. Magn. Reson. 155 (2002) 300–306.
[25] M.J. Duer, Introduction to Solid-state NMR Spectroscopy, Blackwell Science, Oxford, 2004.
[26] J. Herzfeld, A.E. Berger, Sideband intensities in NMR spectra of samples spinning at the magic angle, J. Chem. Phys. 73 (1980) 6021–6030.
[27] M.M. Maricq, J.S. Waugh, NMR in rotating solids, J. Chem. Phys. 70 (1979) 3300–3316.
[28] D. Fenzke, B. Maes, H. Pfeifer, A novel method to determine the principal values of a chemical shift tensor from MAS NMR powder spectra, J. Magn. Reson. 88 (1990) 172–176.
[29] A.C. Olivieri, Rigorous statistical analysis of errors in chemical-shift-tensor components obtained from spinning side bands in solid-state NMR, J. Magn. Reson. Ser. A 123 (1996) 207–210.
[30] D. Vega, R. Baggio, M.T. Garland, Monosodium 4-amino-1-hydroxy-1,1-butanediphosphonate trihydrate (Alendronate), Acta Crystallogr. 52 (1996) 2198–2201.
[31] D. Vega, D. Fernandez, J.A. Ellena, Disodium pamidronate, Acta Crystallogr. 58 (2002) m77–m80.
[32] Y. Pan, T. Gullion, J. Schaeffer, Determination of C-N internuclear distances by rotational-echo double-resonance NMR in solids, J. Magn. Reson. 90 (1990) 330–340.
[33] V. Raghunathan, J.M. Gibson, G. Goobes, J.M. Popham, E.A. Louie, P.S. Stayton, G.P. Drobny, Homonuclear and heteronuclear NMR studies of a statherin fragment bound to hydroxyapatite crystals, J. Phys. Chem. 110 (2006) 9324–9332.
[34] V.M. Coiro, D. Lamba, Structure of 6-amino-1-hydroxyhexylidenebis(phosphonic acid), Acta Crystallogr. 45 (1989) 446–448.